The growth of localized disturbances in a laminar boundary layer

By WILLIAM O. CRIMINALE, JR.* AND
LESLIE S. G. KOVASZNAY

Department of Mechanics, The Johns Hopkins University, Baltimore

The classical theory of the instability of laminar flow predicts the growth (or decay) rate and phase velocity of two-dimensional small disturbance waves. In order to study the growth and dispersion of an originally localized spot-like disturbance, the initial disturbance is built up from all possible simple-harmonic waves. The propagation velocity and amplification rate for each vector wave-number then follows from the two-dimensional theory by Squire's generalization. The initial development can be solved explicitly by a power series in time, and the asymptotic behaviour is also predicted. For times between initial and final periods, exact numerical calculations have been made using an IBM 709 electronic computer. The role which localized disturbances can play in ultimate transition to turbulent motion is also indicated.

1. Introduction

The classical laminar-flow instability theories were developed with the assumption of two-dimensional disturbances. Squire (1933) has shown that, at least for the incompressible case, the development of three-dimensional (oblique) disturbances can be predicted from the corresponding two-dimensional problem at a reduced Reynolds number. For the boundary layer, as indeed for all real parallel flows, the oblique disturbances have a higher critical Reynolds number, and consequently theoretical interest in the problem of three-dimensional instability subsided for a while. On the other hand, recent experimental evidence (Klebanoff & Tidstrom 1959) emphasizes the three-dimensional character of transition, and also points to the pre-existence of three-dimensional disturbances long before actual transition occurs.

Two salient points emerge from a re-examination of the question of three-dimensional disturbances. One is that the amplification factors have only a very broad peak for the two-dimensional disturbances; consequently the slightly oblique waves can still form highly amplified three-dimensional wave packets. The other is that the oblique waves contribute a vorticity component in the direction of the mean flow which in turn interacts quite effectively with the mean vorticity of the boundary layer. In this way an important mechanism is available for the non-linear development of the vorticity component perpendicular to the

* Present address: Department of Mechanical Engineering, Princeton University, Princeton, New Jersey.

wall boundary (Kovasznay 1960), a mechanism that is absent in strictly two-dimensional flows.

Against this background, it was therefore natural to attempt the exploration of a small, initially concentrated pulse-like disturbance as it evolves according to the linear theory. The most important questions were: how rapidly is the pulse-like character of the disturbance lost, and how rapid is the approach toward the ultimately two-dimensional wave packet? In this sense, the present work is more of a heuristic approach.

The initial disturbance was taken as a circular Gaussian pulse. The standard deviation was chosen sufficiently small compared to the most amplified wavelength so that the Fourier spectrum of the disturbance is practically constant (as that of the Dirac function) within the wave-number range of amplified waves. A Dirac 'delta function' could have been chosen, but this function is the same as the limiting case of a Gaussian distribution.

From Squire's theorem and the work of Watson (1960), it can be seen that the most amplified wave will ultimately dominate, and so it was found useful in the later development to normalize all variables with respect to the wavelength of the most amplified wave and not with respect to the boundary-layer thickness.

The results of this work were first presented by Criminale (1960). After the present paper was submitted for publication a related problem was treated by Benjamin (1961) concerning the growth of a localized disturbance in an unstable liquid film and leading to general results that are not inconsistent with our more comprehensive analysis.

2. The classical stability problem

The laminar-flow instability problem is expressed mathematically as a combined initial-value, boundary-value problem. The attention here will be confined to the case of a laminar boundary layer over a flat plate with the time-independent solution due to Blasius. Now assume that, at a time $t = 0$, the boundary layer is subjected to a localized three-dimensional disturbance. In order to study such an event, two assumptions are introduced. First, the disturbance will be considered weak enough so that the equations of motion can be linearized through the use of a perturbation technique. Secondly, the boundary layer will be taken as one of constant thickness.* The growth or decay of the disturbance in time will then be computed.

The classical instability theory was developed in just such a manner as outlined above but with the additional assumption of two-dimensional periodic disturbances. (For a full account see Lin 1955.) Squire (1933) has proven, however, that every three-dimensional (oblique wave) disturbance is equivalent to a two-dimensional disturbance at a lower Reynolds number. Hence, the coupling of this theorem with the results of the purely two-dimensional problem provides a means for solving the three-dimensional problem.

For the boundary layer on the flat plate, the co-ordinate system is chosen so

* In §7C the downstream growth of the boundary-layer thickness is included by permitting δ to increase stepwise. This refinement did not, however, modify the results to an important degree.

that x' is parallel to the undisturbed flow and positive downstream, z' is parallel to the surface and to the leading edge, and y' is normal to the surface and positive only. In the undisturbed state there is only one velocity component, $U'(y')$,
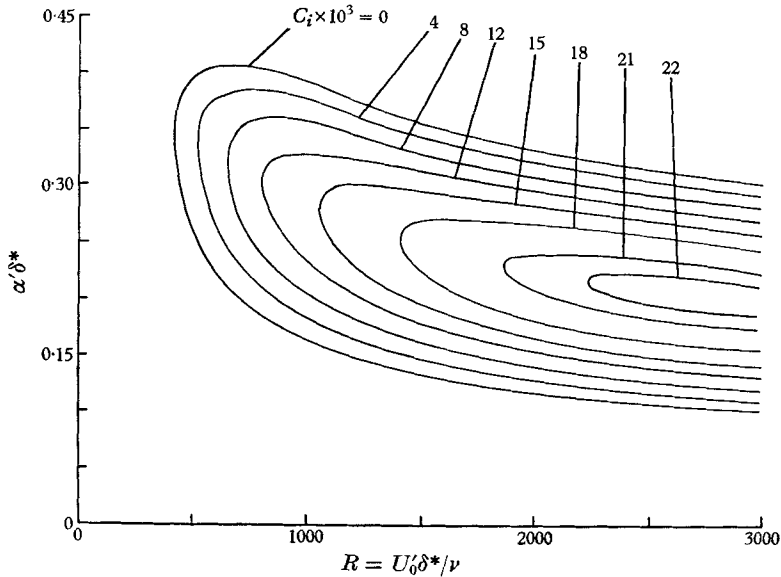

FIGURE 1. Constant amplification rates of two-dimensional disturbance in Blasius boundary layer (after Shen 1954).
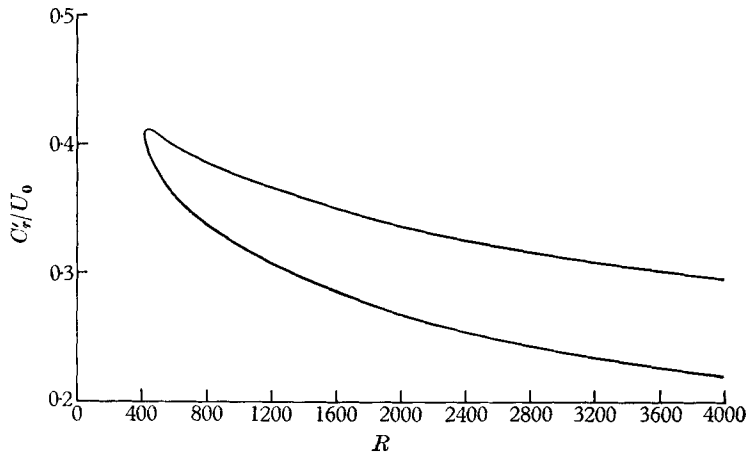

FIGURE 2. Constant phase velocity for neutral two-dimensional disturbance in Blasius boundary layer (after Zaat 1958).

which is in the flow direction. The disturbance velocity components corresponding to x', y', z' are denoted by u', v', w', which are functions of x', y', z' and time t, respectively. The total disturbed velocity at any time is the vector sum of these three components and that of the undisturbed motion. With a two-dimensional system, the w' component and the dependence on z' are missing.

Proceeding in the classical manner, then, a stream function $\psi'(x', y', t)$ can be introduced such that
$$u' = \partial\psi'/\partial y', \quad v' = -\partial\psi'/\partial x'. \tag{2.1}$$

A single partial differential equation results which admits solutions in the form
$$\psi'(x', y', t) = \phi'(y')\, e^{i\alpha'(x'-C't)}, \tag{2.2}$$

where α' is the real wave-number (chosen arbitrarily) and C' is the complex wave velocity. The real part of C' is the phase velocity, and the imaginary part gives the amplification factor. It is the usual convention that only the real part of ψ' is significant for the physical problem.

With the solution (2.2) the system reduces to a fourth-order ordinary differential equation known as the Sommerfeld–Orr equation of instability theory. Applying the boundary conditions to the set of formal solutions leads to an eigenvalue problem where the complex quantity $C = C'/U_0'$ is a function of $\alpha = \alpha'\delta^*$ and $R = U_0'\delta^*/\nu$. (All quantities have been non-dimensionalized with respect to U_0' the free-stream velocity, δ^* the boundary-layer displacement thickness, and ν the kinematic viscosity.) According to whether the imaginary part of C is positive or negative, the disturbance is unstable or stable. The boundary between the stable and unstable domain is the neutral-stability curve where C is real. The results are shown in figures 1 and 2.

3. Formal solution of the three dimensional problem

Using the solution of the classical problem, solutions of the complete system (with w' and z' retained) can be found by using Fourier decomposition, viz.
$$\tilde{u}'(\beta', \gamma'; y', t) = \frac{1}{(2\pi)^2} \int_{-\infty}^{+\infty} \int_{-\infty}^{+\infty} u'(x', y', z', t)\, e^{-i(\beta'x' + \gamma'z')} dx'\, dz', \tag{3.1}$$

with similar expressions for $\tilde{v}'$, $\tilde{w}'$ and $\tilde{p}'$. The inverse transforms are
$$u'(x', y', z', t) = \int_{-\infty}^{+\infty} \int_{-\infty}^{+\infty} \tilde{u}'(\beta', \gamma'; y', t)\, e^{i(\beta'x' + \gamma'z')} d\beta'\, d\gamma', \tag{3.2}$$

and similar expression for v', w' and p'.

Now consider all quantities non-dimensionalized with respect to U_0' and β_0', the latter being the most amplified wave-number. This choice appears more convenient than normalization with the boundary-layer displacement thickness.

The general solution of the three-dimensional problem has other limitations, of course. The initial disturbance must still satisfy the continuity equation and the boundary conditions. Since the co-ordinate y has not been transformed, β, γ and U are not constants but functions of y, and a set of differential equations in y must be still satisfied. It is an important simplification if the initial disturbance is not an arbitrary function of y, but is built up from the eigenfunctions of the Sommerfeld–Orr equation. In that case the particular solutions of the system are (with $\tau = U_0'\beta_0't$)
$$\tilde{u}(\beta, \gamma; y, \tau) = \hat{u}(\beta, \gamma; y)\, e^{-i\beta c\tau}, \tag{3.3}$$

and similar forms for $\tilde{v}$, $\tilde{w}$ and $\tilde{p}$, where c is a complex function of β, γ, $\mathscr{R}$ (see below for $\mathscr{R}$). The real and imaginary parts have the same meaning as given for C, but β, γ, c are not functions of y any more. By abandoning the arbitrary dependence on y in the initial value problem, one has only the eigenfunctions of the

Sommerfeld–Orr problem available. Of course, if a complete orthonormal set of eigenfunctions were available, arbitrary initial conditions could be chosen. Unfortunately, the higher modes of the eigenfunctions for the Sommerfeld–Orr problem have never been computed; indeed their general properties are unknown, so that the problem must be restricted in this sense.

Then, with Squire's substitutions

$$\alpha^2 = \beta^2 + \gamma^2, \tag{3.4}$$

$$\alpha R = \beta \mathscr{R}, \tag{3.5}$$

$$C = c, \tag{3.6}$$

a set of particular solutions can be obtained

$$\hat{v} = [-i\alpha\phi]_{\alpha = (\beta^2 + \gamma^2)^{\frac{1}{2}}, \ R = (\beta/\alpha)\mathscr{R}}, \tag{3.7}$$

$$\hat{u}\cos\theta + \hat{w}\sin\theta = \left[\frac{d\phi}{dy}\right]_{\alpha = (\beta^2 + \gamma^2)^{\frac{1}{2}}, \ R = (\beta/\alpha)\mathscr{R}}, \tag{3.8}$$

where $\phi(y, \alpha, R)$ is the solution of the two-dimensional problem and

$$\theta = \tan^{-1}(\gamma/\beta). \tag{3.9}$$

Squire's conclusions easily follow, if we remember that R is always smaller than $\mathscr{R}$.

The three-dimensional problem has now been completely reduced to the two-dimensional problem, and the latter is assumed to have been solved. More detail is given by Criminale (1960).

4. The equivalent membrane problem

The eigenfunctions and the eigenvalues are all assumed to be known for the two-dimensional problem, and they are used for the solution of the three-dimensional problem. In fact, surprisingly few eigenfunctions have ever been computed even though papers have been written about the subject for more than thirty years. Specifically, the eigenvalues that have actually been computed are for the first mode alone (i.e. the data shown in figures 1 and 2), and only a very few of the eigenfunctions have ever been computed. To the authors' knowledge, the only eigenfunctions that have been computed for the Blasius boundary layer are the two examples due to Schlichting (1935).

The known eigenfunction of the first mode,* $\phi(y)$, is a single lobe curve (having no zero crossings for finite y). The corresponding $v(y)$ normal-velocity distribution is similar in shape and reaches a very broad maximum in the outer part of the boundary layer. The $u(y)$ component has both a positive maximum and negative minimum. These disturbances are superimposed on a mean flow $U(y)$ (see figure 3). If the stream function for the mean flow is defined by

$$\Psi(y) = \int_0^y U(\bar{y})\,d\bar{y},$$

it is clear that with the superimposed disturbances having the stream function defined by (2.1), the instantaneous y-position of a given streamline will oscillate in time. In the outer half of the boundary layer where the broad peak of ϕ and also of v occur, the amplitude of the oscillation of the streamline position in the

* A more thorough discussion of this subject can be found in Grohne (1954).

y-direction will be almost constant (only a slowly varying function of y). In other words, if one specifies the normal velocity v in the outer portion of the boundary layer, this is not very sensitive to the actual choice of distance from the wall.

If it is further assumed that the general shape of the eigenfunctions as plotted against y is similar for different eigenvalues (α and C), then this pulsation of the streamline position in the outer portion of the boundary layer can serve as a new variable and it can be visualized as the oscillation of an 'equivalent membrane'.
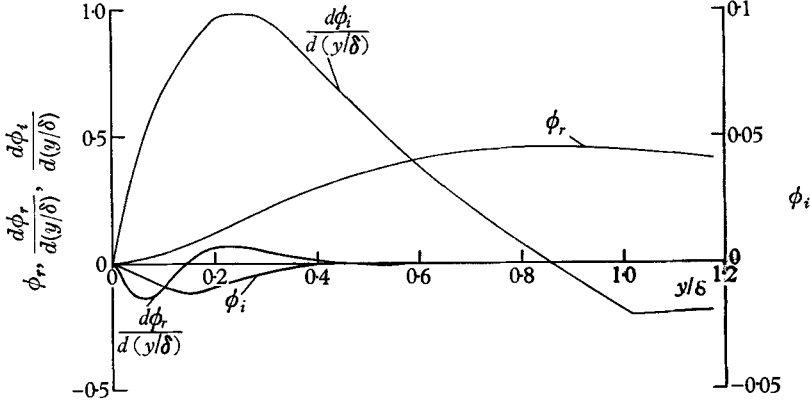

FIGURE 3. Eigenfunction for two-dimensional disturbance in laminar boundary layer for first neutral vibration (after Schlichting 1935).

The normal displacement velocity (y-direction) of a two-dimensional membrane is considered now as the relevant variable, and the actual detailed distribution of v-velocity across the boundary layer will be ignored. Such a description would be rigorously correct only if all eigenfunctions were identical.

The membrane velocity is defined by

$$V(x, z, \tau) = [v(x, y, z, \tau)]_{y=y_1},$$

it being specified that $y = y_1$ where $\partial v/\partial y = 0$ ($y_1'/\delta = 0.8$ for practical purposes).

It would be very difficult to derive the differential equation governing $V(x, z, \tau)$ in physical space and time, but it is relatively easy to obtain it in Fourier-transform variables. From the definition of transform relations

$$\hat{V}(\beta, \gamma, \tau) = \frac{1}{(2\pi)^2} \int_{-\infty}^{+\infty} \int_{-\infty}^{+\infty} V(x, z, \tau)\, e^{-i(\beta x + \gamma z)}\, dx\, dz, \qquad (4.1)$$

$$V(x, z, \tau) = \int_{-\infty}^{+\infty} \int_{-\infty}^{+\infty} \hat{V}(\beta, \gamma, \tau)\, e^{+i(\beta x + \gamma z)}\, d\beta\, d\gamma, \qquad (4.2)$$

the propagation of $\hat{V}(\beta, \gamma, \tau)$ is simply obtained as

$$\hat{V}(\beta, \gamma, \tau) = \hat{V}(\beta, \gamma, 0)\, e^{-i\beta c(\beta, \gamma)\tau}, \qquad (4.3)$$

where equations (3.4), (3.5) and (3.6) give the correspondence with the two-dimensional problem.

Consider now as initial condition a Gaussian pulse located at x_0, z_0. At this location, let the membrane disturbance at $\tau = 0$ be given as

$$V(x, z, 0) = \frac{1}{2\pi\sigma^2} \exp\left\{ -\frac{(x - x_0)^2 + (z \pm z_0)^2}{2\sigma^2} \right\}, \qquad (4.4)$$

where σ is the (non-dimensionalized) standard deviation.

By applying (4.1), we find

$$\hat{V}(\beta, \gamma, 0) = \frac{1}{(2\pi)^2} \exp\left\{ -\tfrac{1}{2}\sigma^2(\beta^2 + \gamma^2) + i(\beta x_0 + \gamma z_0) \right\}. \qquad (4.5)$$

Then, by substituting (4.5) into (4.3) and using the inverse transform given in (4.2), we can write the result for any positive time as

$$V(x, z, \tau) = \frac{1}{(2\pi)^2} \int_{-\infty}^{+\infty} \int_{-\infty}^{+\infty} e^{-\frac{1}{2}\sigma^2(\beta^2 + \gamma^2)} e^{-i\beta c\tau} e^{i(\beta\bar{x} + x\bar{z})} \, d\beta \, d\gamma, \qquad (4.6)$$

where $c = c(\beta, \gamma)$ is the complex phase velocity (it is a function of the wave numbers β, γ). Also $\bar{x} = x - x_0$, $\bar{z} = |z \pm z_0|$; i.e. the co-ordinate system is thus displaced to the location of the initial disturbance.

5. Extension of the available eigenvalues

Using the transformation relations (3.4)–(3.6), the familiar stability curves, which result from the two-dimensional approach, now become surfaces with the addition of one more variable. In order to present the eigenvalue c analogously, one makes a cut of this surface for a constant value of the Reynolds number $\mathcal{R}$. These curves are then projected into the (β, γ)-plane. The most amplified wave is, of course, the one in the direction of the mean flow, according to Squire's conclusions that two-dimensional disturbances are most amplified.* At the same time, however, it should be noted that near the most amplified vector wave-number there is a rather flat-peak amplification region. Figure 4 shows three graphs for $\mathcal{R} = 700, 1300, 2300$; here c_i is a function of $\beta_0' \delta^*$. Figure 5 gives the corresponding graphs for c_r as a function of the same variables.

The details of obtaining the 'kidney' curves of figure 4 and the accompanying phase velocity plots of figure 5 are quite simple. Figure 1 is cross-plotted by varying the angle θ to obtain the results as given in figure 4. The phase velocity is obtained in the same fashion.

The lower critical Reynolds number can be translated into a maximum angle denoted by $\theta_{\max}$, and is given by the relation

$$\theta_{\max} = \cos^{-1}[R_{cr}/\mathcal{R}], \qquad (5.1)$$

indicating that there are no amplified waves more oblique than this value.

---

* This conclusion differs somewhat from the work of Watson (1960), who also computed generalized eigenvalues for three-dimensional disturbances. The fact is, at least so far as it is known, there are no closed amplification curves for the Blasius boundary layer (although there are in the case of plane Poiseuille flow). Hence the point of maximum amplification is *always* the one corresponding to a pure two-dimensional wave.

It is convenient to use an approximate analytical expression for c_i and c_r. If a Taylor expansion is made around the point of maximum amplification for both c_r and c_i as a function of wave-number, and only terms no higher than second order are retained, the results can be written as

$$\frac{c_r'}{U_0'} = \frac{c_{r0}'}{U_0'} + a_1'(\beta'\,\delta^* - \beta_0'\delta^*) + a_2'(\gamma'\delta^*)^2, \tag{5.2}$$

and

$$\frac{c_i'}{U_0'} = \frac{c_{i0}'}{U_0'} - b_1'(\beta'\delta^* - \beta_0'\delta^*)^2 - b_2'(\gamma'\delta^*)^2, \tag{5.3}$$
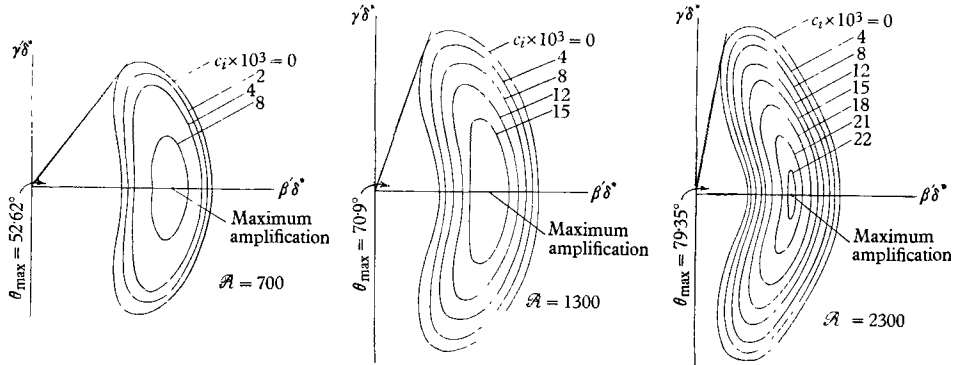
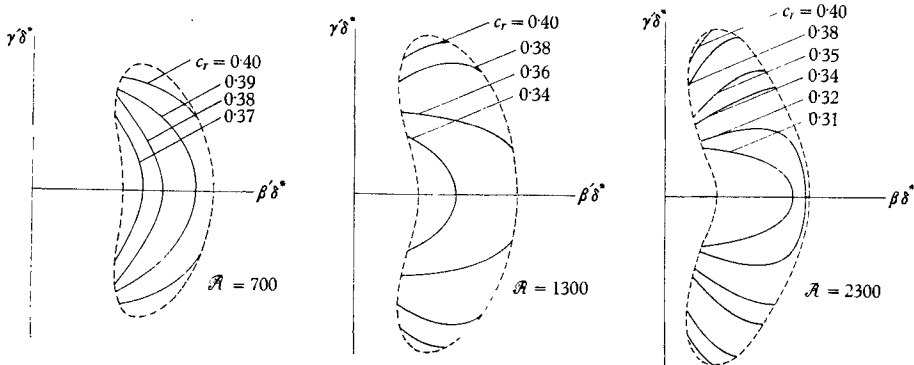FIGURE 4. 'Kidney' curves of constant amplification for oblique waves (cross plotted from figure 1).

FIGURE 5. Constant phase velocity curves for oblique amplified waves.

where the coefficients a_1', a_2', b_1', b_2' are all positive and, in general, functions of the Reynolds number. It is clear that (5.3) replaces the 'kidney' curves of figure 4 by ellipses and (5.2) replaces the curves in figure 5 by parabolas.

It is now more convenient to eliminate δ^* from the equations

$$c_r = c_{r0} + a_1(\beta - 1) + a_2\gamma^2 \tag{5.4}$$

and

$$c_i = c_{i0} - b_1(\beta - 1)^2 - b_2\gamma^2, \tag{5.5}$$

where

$$c_r = c_r'/U_0', \qquad c_i = c_i'/U_0',$$
$$\left.\begin{array}{l} a_1 = a_1'(\beta_0'\,\delta^*), \quad a_2 = a_2'(\beta_0'\,\delta^*)^2, \\ b_1 = b_1'(\beta_0'\,\delta^*)^2, \quad b_2 = b_2'(\beta_0'\,\delta^*)^2. \end{array}\right\} \tag{5.6}$$

The quantity δ^*, is, of course, retained implicitly in $\mathscr{R}$ and the product $(\beta_0'\,\delta^*)$.

6. General features of the wave packet

Unfortunately, closed-form results cannot be obtained for the Fourier integral, even with the use of the approximate functions given in (5.4) and (5.5). On the other hand, the overall behaviour of the disturbance in time can be examined in wave-number space. Hence, without actually performing the integration, a great deal can be learned by merely inspecting the time behaviour of the integrand in (4.6). In turn, salient qualitative features in physical space become evident.

The dependence on the Reynolds number is implicit in the Fourier integral formula, and its effect is small so that it can be treated more as a slowly varying parameter and not as an independent variable. (Note that $\mathscr{R}$ enters only through the function $c(\mathscr{R})$, the complex eigenvalue.) An indication of its effect can be given by examining the order of magnitude of the variation of phase velocity. Define a time T as the value of τ for which the ratio $c'_{r0}t/\lambda'_0$ is equal to unity. This is the time needed by the most amplified wave to travel one wavelength. Typical values of T are given in the accompanying table.

$\mathscr{R}$	T/τ
500	15·84
900	17·08
1500	18·80

Then, in general, the time scale depends somewhat upon Reynolds number at the initial location of disturbance, but the Reynolds number dependence is still rather weak.

The integral in (4.6) can be rewritten as a cosine transform (the wave packet being symmetrical with respect to the $z = z_0$ plane)

$$V = \frac{1}{\pi} \int_0^\infty \int_0^\infty e^{-\frac{1}{2}\sigma^2(\beta^2+\gamma^2)} a^{\beta c_i \tau} \cos\beta\,(\bar{x} - c_r \tau) \cos\gamma\bar{z}\, d\beta\, d\gamma. \tag{6.1}$$

By temporarily abandoning the Gaussian pulse we can find the first result. There is a maximum angle where $\theta = \theta_{max}$. Substituting the values of (β, γ) at this point, a solution is

$$V_N = A_N \cos\beta_N(\bar{x} - c_{rN}\tau) \cos\gamma_N\bar{z}, \tag{6.2}$$

where the subscript N refers to neutral oscillations; i.e.

$$\beta_N = \alpha_N \cos\theta_{max}, \quad \gamma_N = \alpha_N \sin\theta_{max}, \tag{6.3}$$

and
$$A_N = \pi^{-2} \exp\left(-\tfrac{1}{2}\sigma^2\alpha_N^2\right). \tag{6.4}$$
With a change of variables

$$\bar{\bar{x}} = \beta_N(\bar{x} - c_{rN}\tau), \quad \bar{\bar{z}} = \gamma_N\bar{z}, \tag{6.5}$$

it is easy to see that the wave pattern in the $(\bar{\bar{x}}, \bar{\bar{z}})$-plane is the familiar cellular pattern, with standing waves with yaw angles of $\pm\,\theta_N$, given by the relation

$$\theta_N = \tan^{-1}[\bar{\bar{z}}/\bar{\bar{x}}]. \tag{6.6}$$

Returning to the Gaussian pulse, another important result can be obtained if the maximum envelope of the oscillations is considered, without the phase factor. Denoting the (real) amplitude by

$$\hat{A} = e^{-\frac{1}{2}\sigma^2(\beta^2+\gamma^2)} e^{\beta c_i \tau}, \qquad (6.7)$$

the maximum of (6.7) can be found at γ^* and β^*, where

$$\gamma^* = 0 \qquad (6.8)$$

for all time, and

$$\beta^* = \frac{[4b_1 - \sigma^2/\tau] + [(4b_1 - \sigma^2/\tau)^2 + 12b_1(c_{i0} - b_1)]^{\frac{1}{2}}}{6b_1}. \qquad (6.9)$$

(The approximate forms (5.4) and (5.5) have been used for these calculations.) The result of (6.9) has been plotted in figure 6 for two different values of the Reynolds number $\mathscr{R}$. In both cases, the limits $\beta^* \to \beta_{max}$ as $\tau \to \infty$, where computed by assuming that the coefficients in (6.9) are independent of $\mathscr{R}$. As indicated in the graph, the approach to the limiting value is quite rapid.
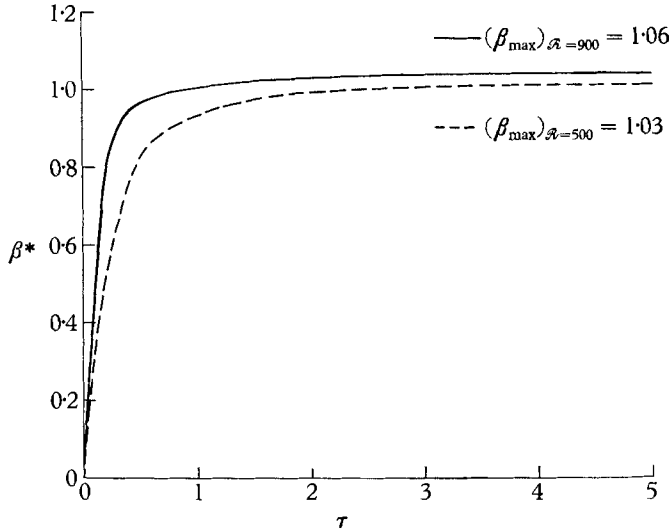

FIGURE 6. Wave space maximum of amplitude $\hat{A}$.

The change of $\hat{A}$ with respect to γ can be determined by computing the second derivatives and evaluating them for the values of (β^*, γ^*). This quantity is

$$\left[\frac{\hat{A}_{\beta\beta}^*}{\hat{A}_{\gamma\gamma}^*}\right]^{\frac{1}{2}} = \frac{\sigma^2/\tau + 2b_1(3\beta^* - 2)}{\sigma^2/\tau + 2b_2\beta^*}, \qquad (6.10)$$

where $\qquad \hat{A}_{\beta\beta}^* = \left[\frac{\partial^2 \hat{A}}{\partial \beta^2}\right]_{\beta=\beta^*, \, \gamma=\gamma^*}, \qquad \hat{A}_{\gamma\gamma}^* = \left[\frac{\partial^2 \hat{A}}{\partial \gamma^2}\right]_{\beta=\beta^*, \, \gamma=\gamma^*}.$

The ratio in (6.10) is plotted in figure 7 for the same two values of $\mathscr{R}$. In real space, the group demodulation corresponds to group spreading, and it is a measure of the lateral transmission of energy compared to the spreading in the flow direction. As was shown in (6.10), the ratio approaches a finite limit for

$\tau \to \infty$. From the limiting values of (6.10) the original 'almost flat' spectrum becomes an elliptical paraboloid centred at the point of maximum amplification with the major axis of the ellipsis parallel to the γ-axis. This much can be surmized also from the 'kidney curves' (figure 4).
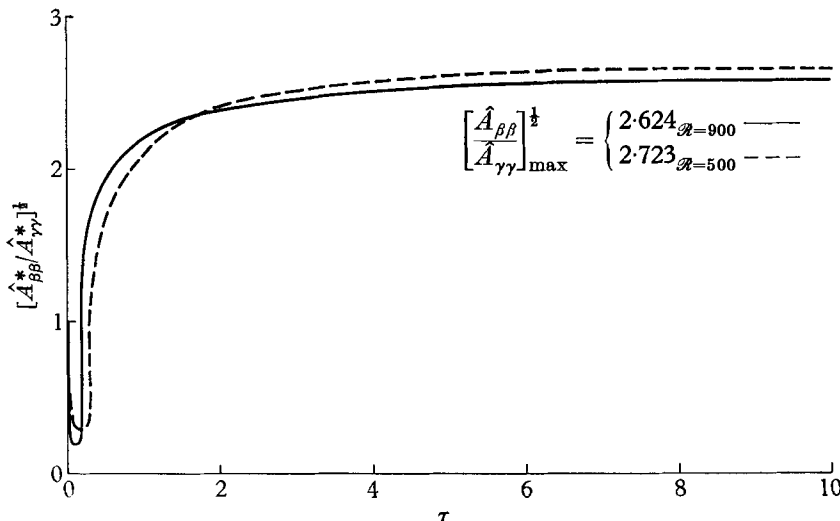

FIGURE 7. Group demodulation.

In physical space it can be inferred that the original small circle becomes an elliptical patch of most amplified waves with the major axis of the patch along the x-axis, having a ratio of spreading of approximately 2:5.

Finally, figures 8 and 9 show the computed band widths of $\hat{A}$ measured from the maximum point both in β and γ. The reciprocal values of these give an indication of the number of oscillations in the wave packet. Using the Taylor series expansion of the amplification and setting it equal to zero, we obtain the equations for β and γ

$$[(c_{i0} - b_1) + (4b_1 - \sigma^2/\tau)\beta - 3b_1\beta^2]^2 + (4b_1 - \sigma^2/\tau) - 6b_1\beta = 0, \qquad (6.11)$$

$$\gamma = \pm 1/(\sigma^2 + 2b_2\beta_{\max}\tau)^{\frac{1}{2}}. \qquad (6.12)$$

The results of (6.11) are shown in figure 8 and (6.12) in figure 9. Quite properly, the initial value is $1/\sigma$ for $\tau = 0$, and the band narrows to $\beta_{\max}$ as $\tau \to \infty$. In the transverse direction, γ varies from $\pm 1/\sigma$ for $\tau = 0$, and as time goes to infinity it approaches zero. Again, the combined effect produces, in the limit, the complete disappearance of oblique waves, and there remains only the pure sine wave with the Tollmien-Schlichting most-amplified frequency.

The group velocity of the waves is denoted by c_g. It can be obtained in the usual manner as

$$c_g^* = \left[\frac{\partial \beta c_r}{\partial \beta}\right]_{\beta = \beta^*, \, \gamma = \gamma^*} = c_{r0} + a_1(2\beta^* - 1). \qquad (6.13)$$

For all numerical calculations, σ was chosen to be the same constant value $\sigma = 0.1$; and since $\sigma = \beta_0'\sigma'$, we have $\sigma' = 0.1/2\pi = 0.0159\lambda_0'$. This meets the requirement that the Gaussian pulse is significantly different from zero for only a few percent of the most amplified wavelengths.
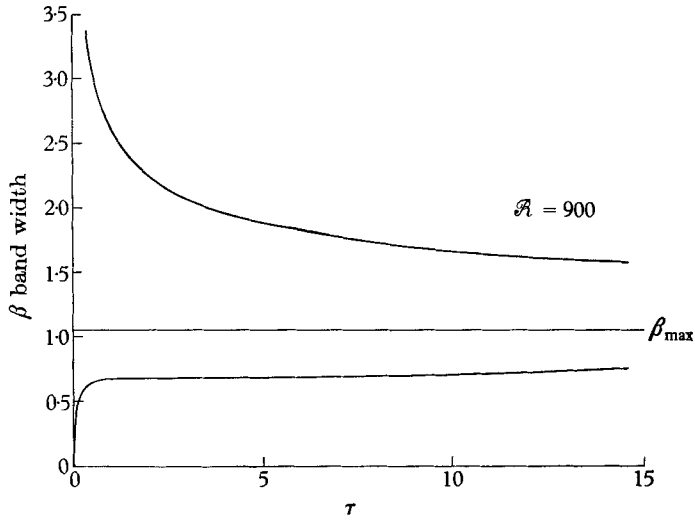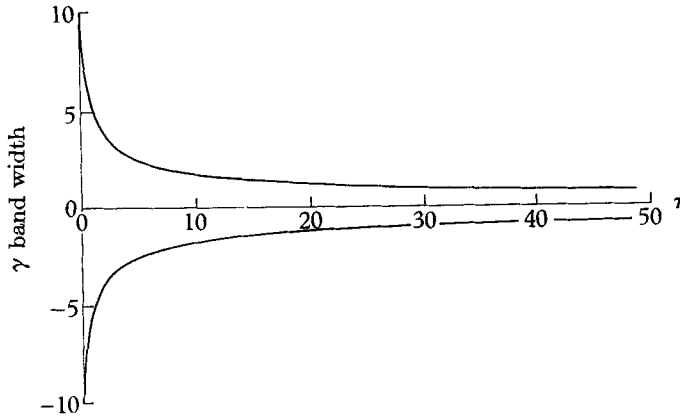
FIGURE 8. Downstream band-width.

FIGURE 9. Lateral band-width.

7. Methods of approximation

A. *Initial period*

A power series expansion for V in time around $\tau = 0$ has the form

$$V = \sum_{l=0}^{\infty} \frac{\tau^l}{l!} \left[\frac{\partial^l V}{\partial \tau^l} \right]_{\tau=0}. \tag{7.1}$$

The function $c(\beta, \gamma)$ can be approximated by the polynomial in β and γ given in (5.4) and (5.5), and the series (7.1) is readily evaluated. Define a complex linear differential operator

$$\mathscr{L} = -\frac{\partial}{\partial i \bar{x}} \bar{c} \left(\frac{\partial}{\partial i \bar{x}}, \frac{\partial}{\partial i \bar{z}} \right), \tag{7.2}$$

where $\bar{c}$ is a linear operator obtained by replacing each β in the polynomial by $\partial/\partial i \bar{x}$ and each γ by $\partial/\partial i \bar{z}$. Using this definition, the expansion for V becomes

$$V = \sum_{l=0}^{\infty} \frac{\tau^l}{l!} [\mathscr{L}^l + \mathscr{L}_*^l] \tfrac{1}{2} V_0, \tag{7.3}$$

where the asterisk indicates the complex conjugate, and V_0 is the value of V at $\tau = 0$; i.e. (4.4) for the present case.

Some calculations for the initial period of distortion are now in order. Expanding (7.3) up to second order in τ gives

$$V = V_0 + \tau \mathscr{L}_r(V_0) + \tau^2 [\mathscr{L}_r - \mathscr{L}_i^2] \tfrac{1}{4} V_0 + \dots, \tag{7.4}$$

where the subscripts r and i refer to the real and imaginary parts of $\mathscr{L}$.

Using the functions (5.4) and (5.5) in (7.2), the operators become

$$\mathscr{L}_r = -(c_{r0} - a_1)\frac{\partial}{\partial \bar{x}} - 2b_1 \frac{\partial^2}{\partial \bar{x}^2} + a_2 \frac{\partial}{\partial \bar{x}}\frac{\partial^2}{\partial \bar{z}^2}, \tag{7.5}$$

$$\mathscr{L}_i = -(c_{i0} - b_1)\frac{\partial}{\partial \bar{x}} + a_1 \frac{\partial^2}{\partial \bar{x}^2} - b_1 \frac{\partial^3}{\partial \bar{x}^3} - b_2 \frac{\partial}{\partial \bar{x}}\frac{\partial^2}{\partial z^2}. \tag{7.6}$$

After performing the prescribed operations and combining terms, the first two terms give

$$V = V_0 \left\{ 1 - \tau \left[\frac{2b_1}{\sigma^4} \bar{x}^2 + \frac{a_2}{\sigma^6} \overline{xz}^2 - [(c_{r0} - a_1)\sigma^2 + a_2] \frac{\bar{x}}{\sigma^4} - \frac{2b_1}{\sigma^2} \right] \right\}. \tag{7.7}$$

By examining (7.7) together with (7.4), information can be extracted without having to resort to numerical work. Up to the values of time that are considered here, it can be noted that neither the maximum amplification value, c_{i0}, nor the coefficient for amplification in the lateral direction b_2 appears yet in the expansion. It is not until terms of the second order in τ are retained that they will have influence. Consequently, the first change is a flattening down of the peak and a spreading out of the distribution. The spread is much greater in the $\bar{z}$-direction than in $\bar{x}$ since σ is present at a higher power in the denominator in the $\bar{z}^2$ term of (7.7). This behaviour was already suggested in § 6.

B. *Asymptotic behaviour for large τ*

Inspection of the integrand in (6.1) showed that as time progresses the original spectrum tends to cluster and become peaked around the point of maximum amplification. It is now possible to approximate the integral for large time by the method of steepest descent.

The product βc is approximated by a quadratic function of β and γ over the amplified wave number region. With (5.4) and (5.5) for the eigenvalue, the product βc is cubic in β. With these substitutions in (6.1), the double integral can be integrated once with respect to γ:

$$V = \frac{1}{2\pi^{\frac{3}{2}}(q_1 \tau)^{\frac{1}{2}}} \int_0^\infty e^{\hat{Q}\tau} \cos \hat{\phi} \, d\beta, \tag{7.8}$$

where
$$q_1^2 = (b_2^2 + a_2^2)\beta_{\max}^2,$$

$$\hat{Q} = -\frac{\bar{z}^2}{\tau^2}\frac{b_2\beta_{\max}}{4q_1^2} + c_{i\max} - B(\beta - \beta_{\max})^2,$$

$$\hat{\phi} = \frac{\bar{z}^2}{\tau^2}\frac{(a_2\beta_{\max})}{4q_1^2}\tau - \tfrac{1}{2}\theta + \beta\bar{x} - [(c_{r0} - a_1)\beta + a_1\beta^2]\tau,$$

$$\theta = \tan^{-1}\left(\frac{a_2}{b_2}\right), \quad B = b_1(3\beta_{\max} - 2).$$

To obtain only the amplified portion of the spectrum, the integration in β will be limited to $\beta_1 < \beta < \beta_2$, the band of amplified region for $y = 0$. The integration is now performed and the final result becomes

$$V \propto \frac{e^{Q\tau}}{4\pi\tau\sqrt{(q_1 q_2)}}\left\{\cos\phi\left[\operatorname{erf}(K_r) - \operatorname{erf}(k_r)\right] - \frac{2}{\sqrt{\pi}}\exp(-K_r^2)\int_0^{k_i} e^{\xi^2}\sin(\phi - 2K_r\xi)\,d\xi\right.$$

$$\left. + \frac{2}{\sqrt{\pi}}\exp(-k_r^2)\int_0^{k_i} e^{\xi^2}\sin(\phi - 2k_r\xi)\,d\xi\right\}, \quad (7.9)$$

where $q_2^2 = B^2 + a_1^2$, and

$$Q = c_{i_{\max}} - B\beta_{\max}^2 - \frac{\bar{z}^2}{\tau^2}\frac{b_2\beta_{\max}}{4q_1^2}$$

$$+ \frac{B}{4q_2^2}\left\{4B^2\beta_{\max}^2 - \left[\frac{\bar{x}}{\tau} - (c_{r0} - a_1)\right]^2\right\}\frac{a_1}{2q_2^2}\left\{2B\beta_{\max}\left[\frac{\bar{x}}{\tau} - (c_{r0} - a_1)\right]\right\},$$

$$\phi = \frac{\bar{z}^2}{\tau^2}\frac{(a_2\beta_{\max})}{4q_1^2}\tau - \frac{(\omega + \theta)}{2}$$

$$+ \frac{B\tau}{2q_2^2}\left\{2B\beta_{\max}\left[\frac{\bar{x}}{\tau} - (c_{r0} - a_1)\right]\right\}\frac{a_1\tau}{4q_2^2}\left\{2B^2\beta_{\max}^2 - \left[\frac{\bar{x}}{\tau} - (c_{r0} - a_1)\right]^2\right\},$$

$$\omega = \tan^{-1}(a_1/B),$$

$$K_r = \tau^{\frac{1}{2}}q^{\frac{1}{2}}\left[\beta_2\cos\left(\frac{\omega}{2}\right) - \frac{r}{2q^2}\cos\left(\chi - \frac{\omega}{2}\right)\right],$$

$$K_i = \tau^{\frac{1}{2}}q^{\frac{1}{2}}\left[\beta_2\sin\left(\frac{\omega}{2}\right) - \frac{r}{2q_1}\sin\left(\chi - \frac{\omega}{2}\right)\right],$$

$$k_r = \tau^{\frac{1}{2}}q^{\frac{1}{2}}\left[\beta_1\cos\left(\frac{\omega}{2}\right) - \frac{r}{2q_1}\sin\left(\chi - \frac{\omega}{2}\right)\right],$$

$$k_i = \tau^{\frac{1}{2}}q^{\frac{1}{2}}\left[\beta_1\sin\left(\frac{\omega}{2}\right) - \frac{r}{rq_1}\sin\left(\chi - \frac{\omega}{2}\right)\right],$$

$$r^2 = (2B\beta_{\max})^2 + \left[\frac{\bar{x}}{\tau} - (c_{r0} - a_1)\right]^2,$$

$$\chi = \tan^{-1}\frac{\bar{x}/\tau - (c_{r0} - a_1)}{2B\beta_{\max}}.$$

The dominating term of the expression is $e^{Q\tau}$, and it decreases as $\exp(-\bar{x}^2)$ for a fixed τ. Each of the two integrals in the brackets can be shown to decay as $\bar{x}^{-1}\exp(-\bar{x}^2)$. The final terms (the error functions) approach unity as $1 - \bar{x}^{-1}\exp(-\bar{x}^2)$.

The location of the maximum amplitude of the asymptotic expression is found to be

$$\bar{z}^* = 0 \tag{7.10}$$

for all τ, and

$$\bar{x}^* = [c_{r0} + a_1(2\beta_{\max} - 1]\tau. \tag{7.11}$$

The rate at which $\bar{x}^*$ is convected downstream is the velocity

$$v_g = c_{r0} + a_1(2\beta_{\max} - 1). \tag{7.12}$$

Both (7.11) and (7.12) have been plotted in figure 10 assuming the disturbance occurred originally at $\mathscr{R} = 500$. This result is compatible with that found in § 6, since v_g agrees with c_g evaluated at $\beta^* = \beta_{\max}$ (6.13). If a particle was released at x_0, z_0 at $\tau = 0$ and it travelled downstream with the phase velocity of the most amplified wave, it would have a position
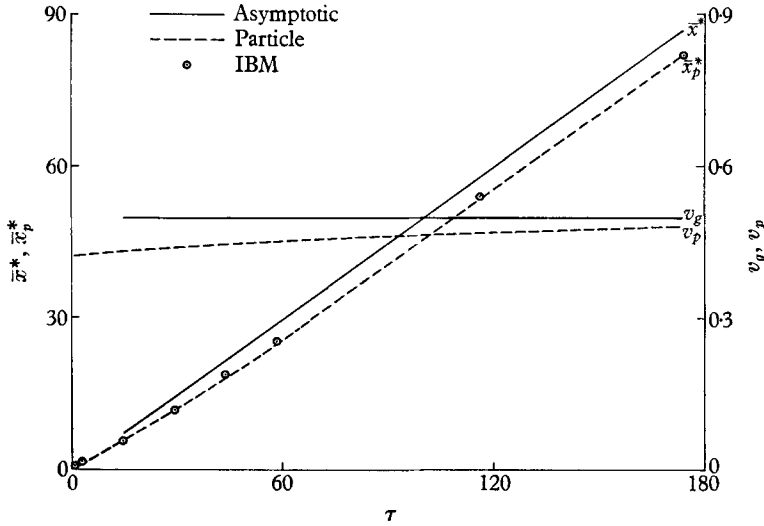
$$\bar{x}_p^* = c_{r0}\tau, \tag{7.13}$$

FIGURE 10. Asymptotic behaviour of wave packet.

and a velocity $v_p = c_{r0}$. The particle would move more slowly than the group velocity (7.12). In figure 10, $\bar{x}_p^*$ and v_p have been entered for comparison.

The asymptotic values for the standard deviation of the wave packet are

$$\sigma_{\bar{x}} = (2\tau)^{\frac{1}{2}} \left[\frac{b_1^2(3\beta_{\max}-2)^2 + a_1^2}{b_1(3\beta_{\max}-2)} \right]^{\frac{1}{2}}, \tag{7.14}$$

$$\sigma_{\bar{z}} = (2\tau)^{\frac{1}{2}} \left[\frac{(b_2^2 + a_2^2)\beta_{\max}}{b_2} \right]^{\frac{1}{2}}. \tag{7.15}$$

The results again show that $\sigma_{\bar{x}} > \sigma_{\bar{z}}$, in agreement with § 6.

Another quantity is connected with group spreading

$$\left[\frac{A_{\bar{z}\bar{z}}}{A_{\bar{x}\bar{x}}} \right]^{\frac{1}{2}} = \left\{ \frac{b_2[b_1^2(3\beta_{\max}-2)^2 + a_1^2]}{b_1 \beta_{\max}(3\beta_{\max}-2)(b_2^2 + a_2^2)} \right\}^{\frac{1}{2}}. \tag{7.16}$$

Its numerical values, for the Reynolds numbers used in § 6, are

$$\left[\frac{A_{\bar{z}\bar{z}}}{A_{\bar{x}\bar{x}}} \right]^{\frac{1}{2}}_{\max} = 3\cdot 29, \quad \mathscr{R} = 500,$$

$$\left[\frac{A_{\bar{z}\bar{z}}}{A_{\bar{x}\bar{x}}} \right]^{\frac{1}{2}}_{\max} = 2\cdot 63, \quad \mathscr{R} = 900.$$

The agreement of (7.16) with the values in figure 7 is much better for the large $\mathscr{R}$ value. This is primarily because of the difference in the limiting expressions

(7.16) and (6.10). For (6.10), the coefficients do not change very much with Reynolds number.

The shape of the maximum wave packet can be illustrated. The major and minor axes of the ellipse are computed and compared to the Tollmien–Schlichting wavelength as

$$\frac{2a'}{\lambda_0} = \epsilon_{\bar{x}} \sqrt{\frac{\bar{x}^*}{\lambda_0}}, \tag{7.17}$$

and

$$\frac{2b'}{\lambda_0} = \epsilon_{\bar{z}} \sqrt{\frac{x^*}{\lambda_0}}, \tag{7.18}$$

where $2a'$, $2b'$ are the major and minor axes of the ellipse. The coefficients $\epsilon_{\bar{x}}$ and $\epsilon_{\bar{z}}$ can be obtained from breaking up the ratio (7.16).

Typical values for the spreading coefficients are

$$\epsilon_{\bar{x}} = 0 \cdot 297, \quad \epsilon_{\bar{z}} = 0 \cdot 0876, \quad \text{for} \quad \mathscr{R} = 500;$$

$$\epsilon_{\bar{x}} = 0 \cdot 226, \quad \epsilon_{\bar{z}} = 0 \cdot 0855, \quad \text{for} \quad \mathscr{R} = 900.$$

These values indicate that the approach to the pure Tollmien–Schlichting wave train is exceptionally slow. For example, if it is assumed that the spot originated at $\mathscr{R} = 900$, then to attain a lateral spread of as much as $10\lambda_0'$, the centre of the group wave packet must move as far as $13,680\lambda_0'$! The asymptotic situation is indicated in figure 11.
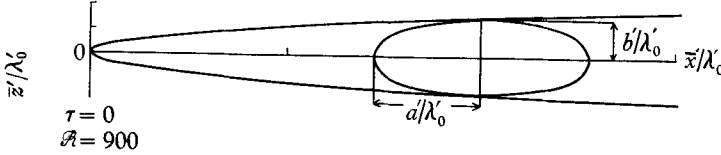

FIGURE 11. Asymptotic wave packet.

The maximum amplitude occurring in the group grows as

$$A_{\max} = \frac{e^{(c_i)_{\max}\tau}}{4\pi\tau\sqrt{(q_1 q_2)}} \approx \frac{e^{(c_i)_{\max}\tau}}{\tau}, \tag{7.19}$$

where $(c_i)_{\max} = c_i(\beta_{\max}, 0)$. The constant phase lines in the wave packet can be found from (7.9) and are controlled by the function $\phi(\bar{x}, \bar{z}^2, \tau)$. Constant phase occurs along $\phi = \Gamma = \text{const}$. From (7.9) it is found that

$$\zeta_1 \frac{\bar{z}^2}{\tau^2} + \zeta_2 \left(\frac{\bar{x}}{\tau} - \mathscr{C}\right) + \zeta_3 \left(\frac{\bar{x}}{\tau} - \mathscr{C}\right)^2 = \frac{(\Gamma + \zeta_4)}{\tau} + \zeta_5, \tag{7.20}$$

representing ellipses in the $(\bar{x}, \bar{z})$-plane, where

$$\zeta_1 = a_2 \beta_{\max}/4q_1^2, \quad \zeta_2 = B^2 \beta_{\max}/q_2^2,$$

$$\zeta_3 = a_1/4q_2^2, \quad \zeta_4 = \tfrac{1}{2}(\omega + \theta),$$

$$\zeta_5 = a_1 B^2 \beta_{\max}^2/q_2^2, \quad \mathscr{C} = c_{r_0} - a_1,$$

$$\left(\frac{\zeta_1}{\zeta_3}\right)^{\frac{1}{2}} = \left(\frac{a_2 q_2^2 \beta_{\max}}{a_1 q_1^2}\right)^{\frac{1}{2}}.$$

Typical values are

$$(\zeta_1/\zeta_3)^{\frac{1}{2}} = 0.802 \quad \text{for} \quad \mathscr{R} = 500, \quad \text{and} \quad (\zeta_1/\zeta_3)^{\frac{1}{2}} = 0.831 \quad \text{for} \quad \mathscr{R} = 900.$$

Since these values are less than unity, the ellipses have their major axes parallel to the $\bar{z}$-axis. Indeed, they are almost circles. It can be concluded, therefore, that within the wave packet, the phasing is locally that of Tollmien–Schlichting waves (two-dimensional waves), but with a sweep-back in $\bar{z}$. (The sweep-back is already clearly discernible in figure 12g).
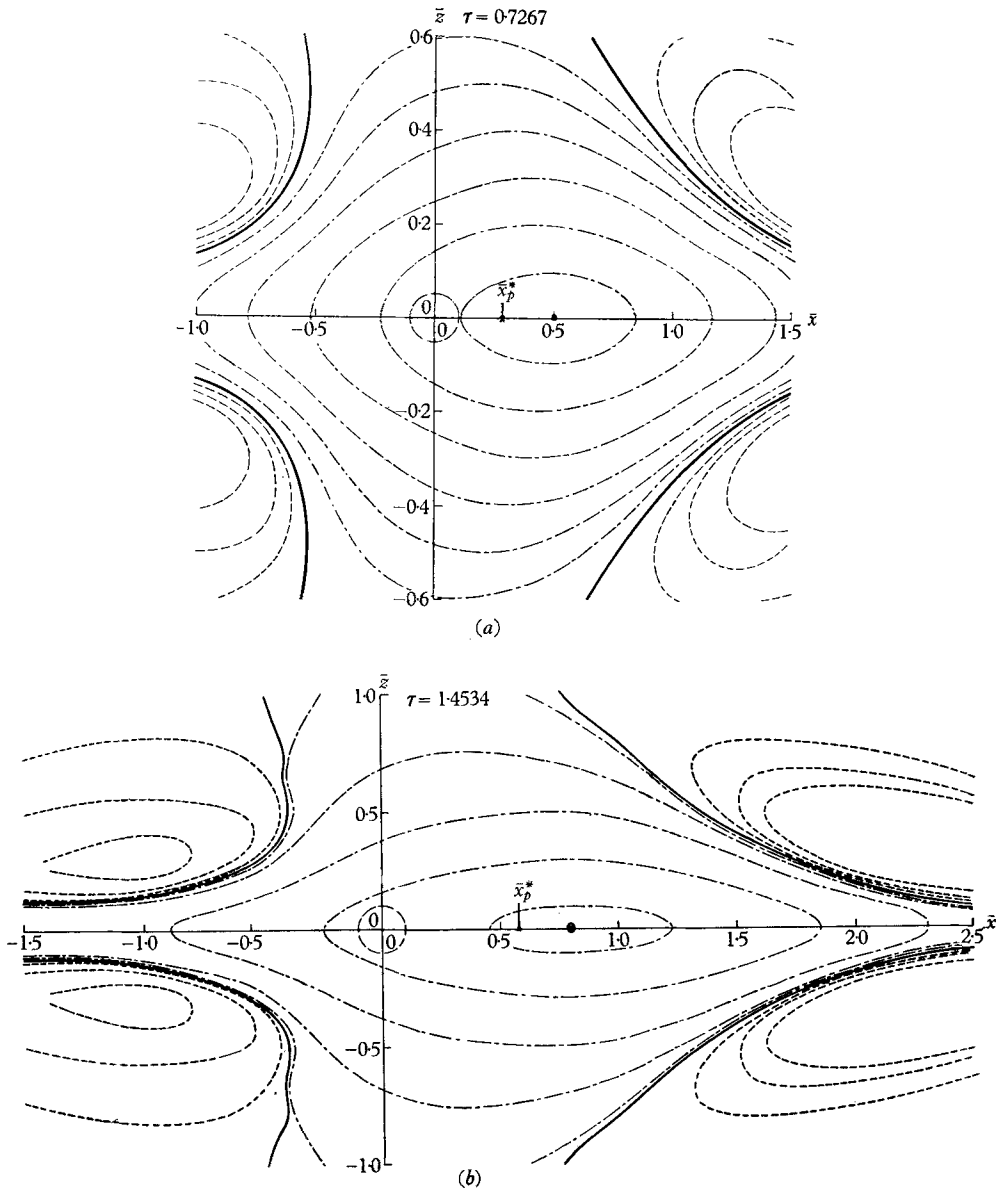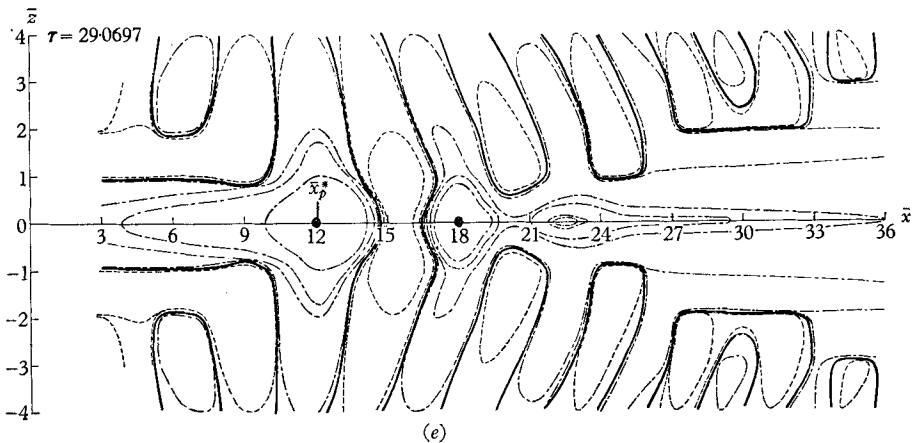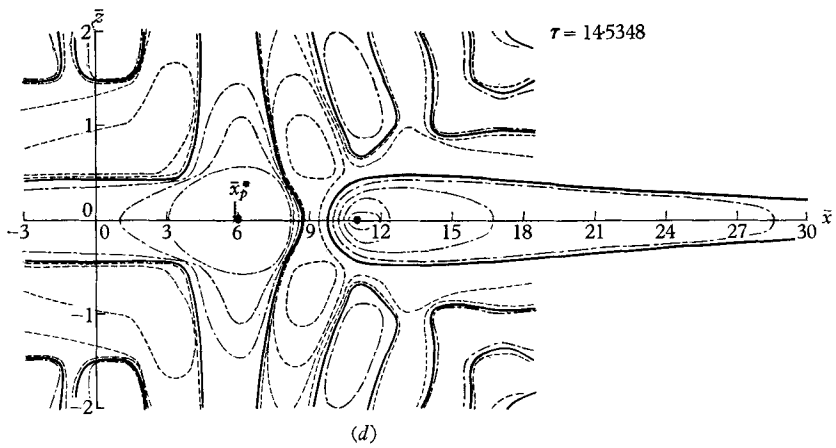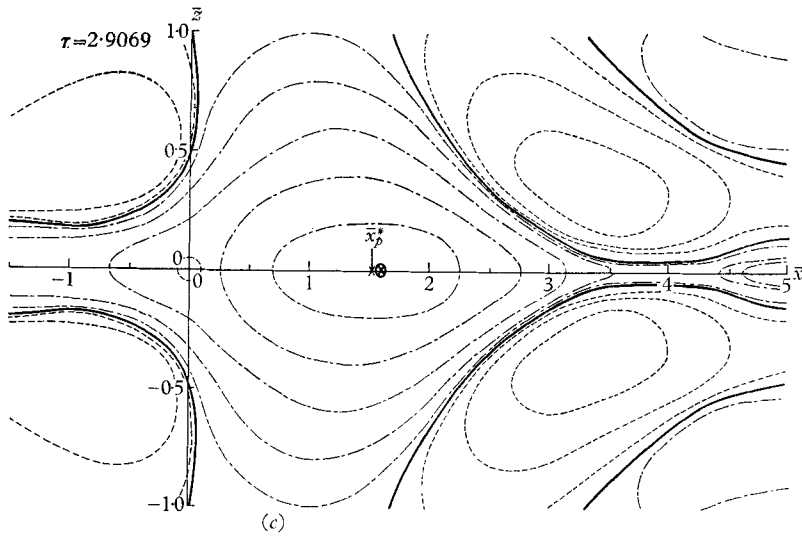
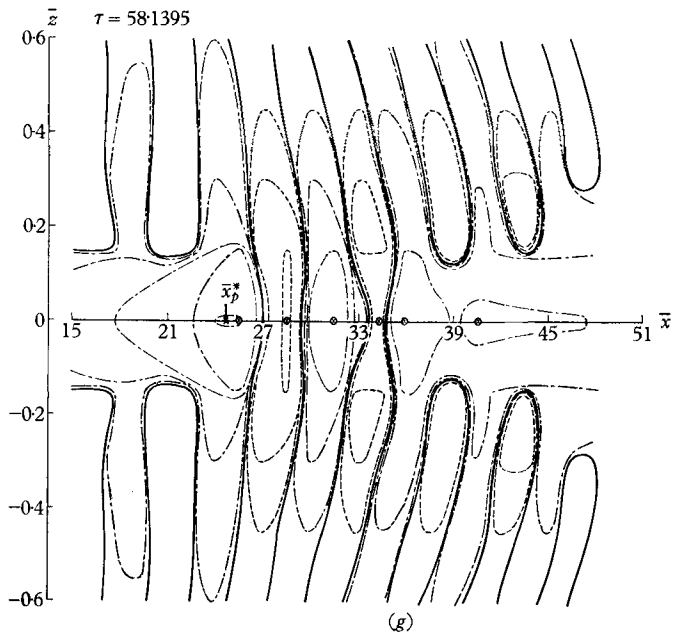FIGURE 12. (For legend see p. 77).

FIGURE 12. (For legend see p. 77).

$\bar{z}$ $\tau = 43 \cdot 6046$

$\bar{x}_p^*$

(f)

$\bar{z}$ $\tau = 58 \cdot 1395$

$\bar{x}_p^*$

(g)

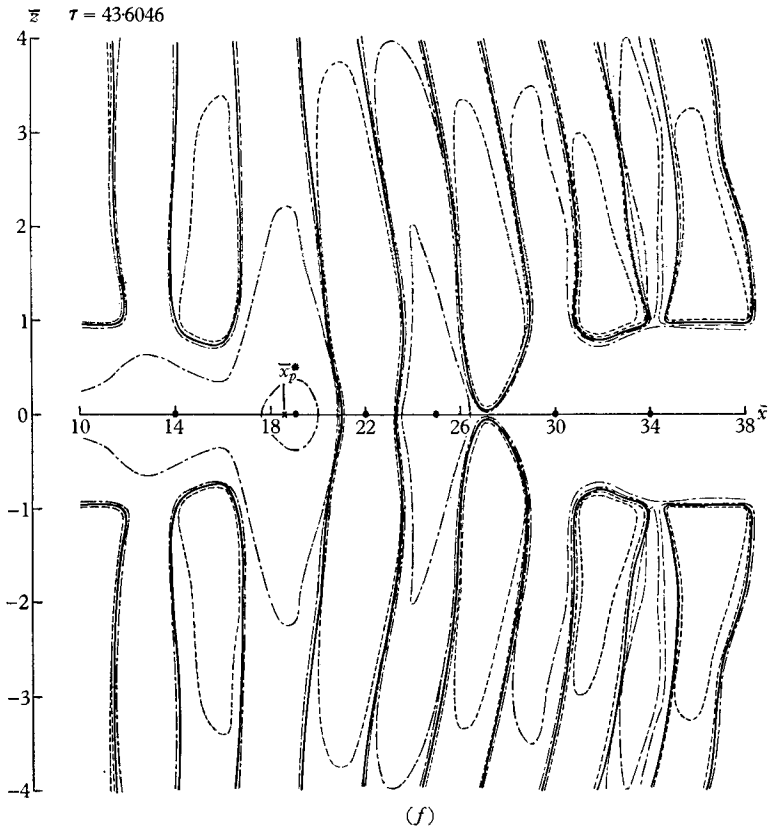FIGURE 12a–g. $----$, $V < 0$; $—$, $V = 0$; $—\cdot—\cdot$, $V > 0$.

C. *Numerical analysis*

There still remains a large gap between the initial period and the asymptotic region. For the values of time between these two periods, results have been obtained by evaluating the integral (6.1) on an IBM 709 electronic computer using the functions (5.4) and (5.5).

The initial disturbance was assumed to be at $\mathscr{R} = 500$. Moreover, since it did not complicate the computation, the Reynolds number growth was also taken into account, by permitting the boundary layer to grow in a stepwise manner. The

$V(\bar{x}, 0, \tau)$

$V(\bar{x}, 0, \tau)$
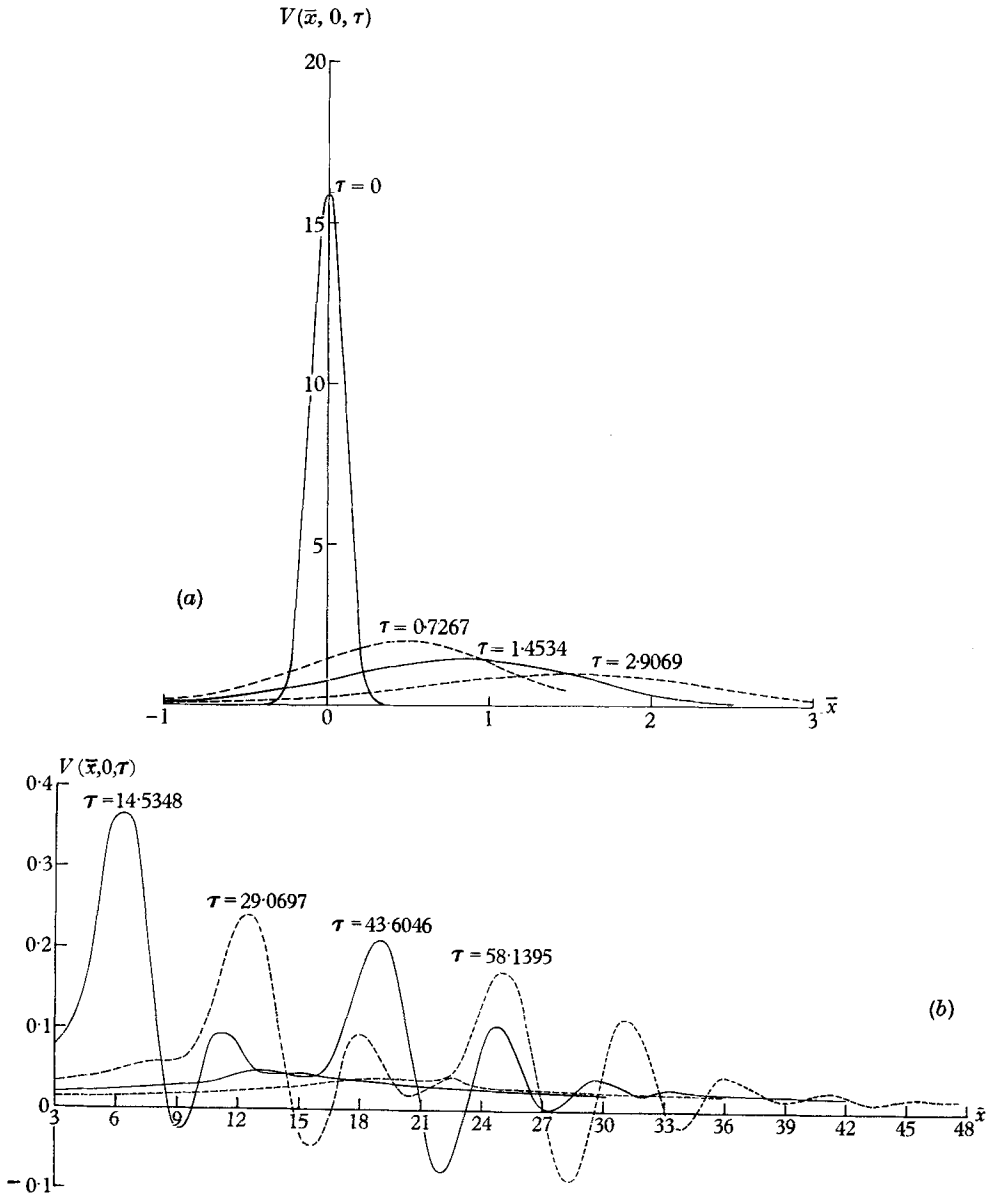
FIGURE 13 *a, b.*

results of the calculations are presented in two ways. First, there are a series of V contour maps (figure 12*a* to 12*g*, each one for a different value of τ). Secondly, $V(\bar{x}, 0)$ along the line $\bar{z} = 0$ is plotted in figure 13*a* and 13*b*.

There is some additional information included in figure 12*a* to 12*g*. On every contour map, $\bar{x}_p^*$, the location of the particle moving with the phase velocity of the most amplified wave, has been marked. For the earlier times the circle of standard deviation of the initial disturbance at the original location has been drawn; as time goes on, the circle gradually becomes a point at the origin owing to the much greater $\bar{x}$ and $\bar{z}$ scale at larger τ values. The addition of the particle location gives, in essence, a running comparison of the location of the pure Tollmien–Schlichting wave and the group wave packet.
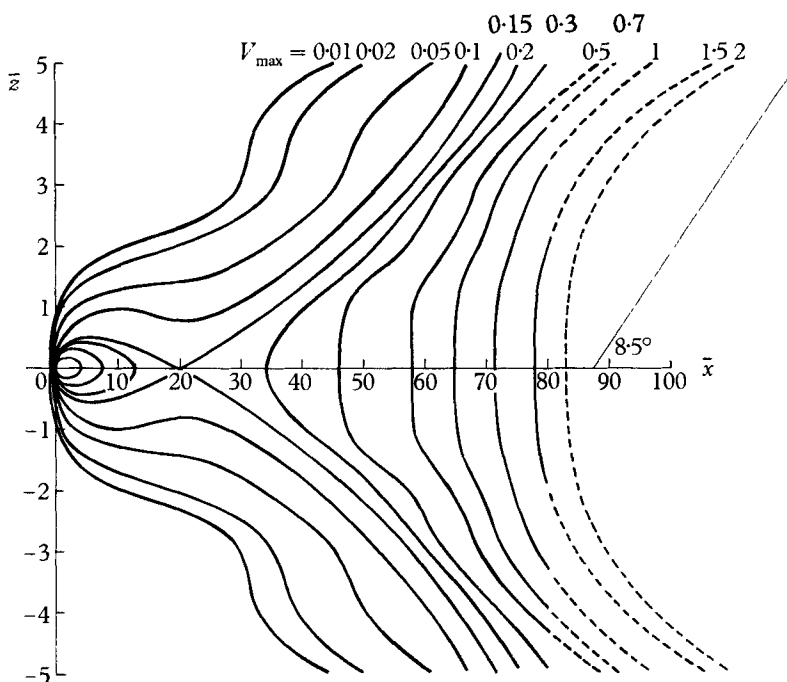

FIGURE 14.

The location of the maximum positive V-amplitude obtained in figures 12*a* to 12*g* has been plotted in figure 10. Except for the initial period the location of the maximum travels for all practical purposes with the phase velocity of the most amplified wave.

Judging from the velocity disturbance plots in figure 13*a* and 13*b*, the conclusion that the group velocity exceeds the particle velocity is correct. The figures clearly indicate that waves are coming in from the downstream side of the packet and then are going out at the rear.

The development of the wave packet can be easily followed in figure 12*a* to 12*g*, and in figure 13*a* and 13*b*. If pulses were released at random intervals from a fixed location $\bar{x} = 0$, $\bar{z} = 0$ the resulting disturbance $V(\bar{x}, \bar{z}, t)$ at any given location $\bar{x}$, $\bar{z}$ would consist of a random sequence of wave trains. The maximum numerical

values of the disturbance $V_{max}(\bar{x}, \bar{z})$ would be attained at different times for every location $\bar{x}, \bar{z}$. This maximum value 'ever attained' for every location $\bar{x}, \bar{z}$ is plotted in figure 14. The scales of $\bar{x}$ and $\bar{z}$ differ by a factor of 10 for convenient presentation of the data. The contours represent logarithmically increasing maximum levels.

There is an isolated maximum at the origin due to the high-peaked initial pulse. A saddle point at $\bar{x} = 20$, $\bar{z} = 0$ separates the decreasing and increasing portion of the disturbance. There is even the suggestion of wedged-shaped spreading, and for reference the average spreading angle of a turbulent spot ($8\cdot5°$) has been indicated (Klebanoff & Tidstrom 1959; Schubauer & Skramstad 1948; Schubauer & Klebanoff 1956). It is not suggested here that the spreading of the wave packet actually represents the behaviour of the turbulent spot. On the other hand, however, the presence of an existing turbulent spot could drive linearly unstable waves laterally into the laminar portion of the layer with a lateral spreading angle that is consistent with present theory.

REFERENCES

BENJAMIN, T. BROOKE 1961 *J. Fluid Mech.* **10**, 401.

CRIMINALE, JR. W. O. 1960 *AGARD Report*, no. 266, *Paris*.

EMMONS. H. W. 1951 *J. Aero. Sci.* **18**, 490.

GROHNE, D. 1954 *ZAMM* **35**, 344.

KLEBANOFF, P. S. & TIDSTROM, K. D. 1959 *NASA TN* D-195.

KOVASZNAY, L. S. G. 1960 *Aeronautics and Astronautics*. London: Pergamon.

LIN, C. C. 1955 *The Theory of Hydrodynamic Stability*. Cambridge University Press.

SCHLICHTING, H. 1935 *Nachrichten von der Gesellschaft der Wissenschaften zu Göttingen*. Neue Folge, Band I, 4.

SCHUBAUER, G. B. & SKRAMSTAD, H. K. 1948 *NACA Rep.* no. 909.

SCHUBAUER, G. B. & KLEBANOFF, P. S. 1956 *NACA Rep.* no. 1289.

SHEN, S. F. 1954 *J. Aero. Sci.* **21**, 62.

SQUIRE, H. B. 1933 *Proc. Roy. Soc.* A, **142**, 621.

WATSON, J. 1960 *Proc. Roy. Soc.* A, **254**, 562.

ZATT, J. A. 1958 *Numerische Beiträge zur Stabilitätstheorie der Grenschichten*. Berlin: Springer-Verlag.